Correlations of instantaneous transition energy and intensity of absorption peaks during molecular vibration: toward potential hyper-surface

2008 New J. Phys. 10 065015

(http://iopscience.iop.org/1367-2630/10/6/065015)

New Journal of Physics
The open-access journal for physics

Correlations of instantaneous transition energy and intensity of absorption peaks during molecular vibration: toward potential hyper-surface

Takayoshi Kobayashi [1,2,3,4,5] **and Zhuan Wang**[1,2]

[1] Department of Applied Physics and Chemistry and Institute of Laser Science, University of Electro-communications, Chofugaoka 1-5-1, Chofu, Tokyo, 182-8585 Japan
[2] JST, ICORP, Ultrashort Pulse Laser Project, 4-1-8 Honcho, Kawaguchi, Saitama, Japan
[3] Institute of Laser Engineering, Osaka University, Yamadakami 2-6, Suita 565-0871, Ibaraki 567-0047, Japan
[4] Department of Electrophysics, National Chiao Tung University, 1001 Ta Hsueh Road, Hsinchu 3005, Taiwan
E-mail: kobayashi@ils.uec.ac.jp

New Journal of Physics **10** (2008) 065015 (13pp)
Received 29 February 2008
Published 30 June 2008
Online at http://www.njp.org/
doi:10.1088/1367-2630/10/6/065015

Abstract. Time-resolved spectrum after ultrashort pulse excitation revealed fine structure of instantaneous vibronic absorption spectra in a thiophene derivative. The probe photon energy-dependent amplitudes of molecular vibration coupled to the induced absorption were composed of several peaks. An absorbance-change peak-tracking method revealed four vibronic transitions buried in the time-integrated spectra over several vibrational periods of typical molecular vibration. Four vibronic transitions located at 2.024, 1.921, 1.818 and 1.731 eV were found to be correlated among themselves with respect to the photon energies and intensities of the peaks in the difference absorbance change spectra. From the size and sign of the correlation strengths the mechanism of the vibronic coupling was related to non-Condon mechanism and Herzberg–Teller vibronic coupling.

[5] Author to whom any correspondence should be addressed.

Contents

1. Introduction

Following the short pump pulse excitation, a wave packet is prepared by the linear superposition of several vibrational quantum numbers being covered by the spectral width of the pump laser and it moves on the potential energy surface (PES) [1, 2]. The wave packet can be generated either in the excited state via simultaneous coherent excitation of several (at least two) vibrational levels or of those in the ground state via 'impulsive' stimulated Raman scattering (ISRS) [3, 4]. These processes are considered to be an extended version of quantum beats of V-type and Λ-type [5, 6]. The motion of the wave packet modulates the intensity and shape of transition spectra between the ground and excited vibronic states. Thus, the wave packet motion of some vibrational mode can be probed by measuring the time-dependent transient difference absorbance with a weak probe pulse. Utilizing the principle and recently developed ultrashort pulse laser [7]–[16], it has become possible to directly observe the vibrational dynamics and coherence properties of the motion of molecular and solid-state systems through femtosecond real-time spectroscopy [17]–[24]. The vibrational dynamics provide time-resolved molecular structural change taking place in the excited states and intermediate in photochemistry because the vibrational spectra contain the information on structure. It can also be used for the clarification of ultrafast dynamics of molecular levels in molecular devices, such as optical memory, optical switch and light-emitting diode (LED), of which effectiveness is relevant to the molecular structure.

The sample studied in the work is a thiophene derivative. Thiophene oligomers have been studied extensively for their possible applications to organic LEDs (OLEDs), field-effect transistors and nonlinear optical devices [25, 26]. Understanding the relaxation mechanism of the excited state is of vital importance to improve the emissivity of OLEDs. Therefore, it is highly required to study the relaxation dynamics in thiophene oligomers. It is also important and interesting to clarify the mechanism of vibronic coupling, which controls the vibronic spectral shape and radiationless relaxation. The change in the spectral shape induces the imaginary part of the susceptibility χ_i, which in turn modifies the real part χ_r through the Kramers–Kronig relation. The complex susceptibility, $\chi_r + i\chi_i$, after the change is given by $\chi_r + i\chi_i = \chi_r^{(0)} + i\chi_i^{(0)} + (\chi_r^{(3)} + i\chi_i^{(3)})E^2$ under scalar approximation using the real and imaginary parts of the third-order susceptibility, $\chi_r^{(3)}$ and $\chi_i^{(3)}$, respectively. Thus, the change in the spectral shape is expressed in terms of the third-order nonlinearity. The third-order nonlinearity is not

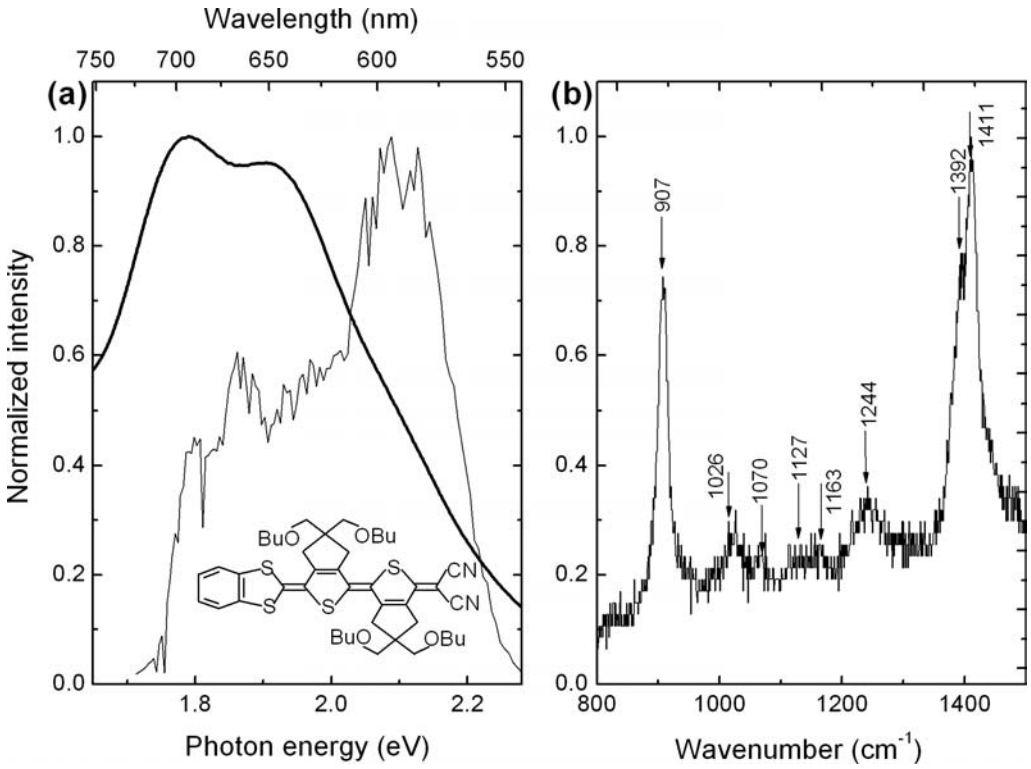

Figure 1. (a) The laser spectrum (thin solid line) and stationary absorption (thick solid line). The inset is the molecular structure used in the present study. (b) The Raman scattering spectrum of the molecule QT2 excited at 514.5 nm (Ar laser).

a stationary one, but it represents the dynamical nonlinearity response of the material. Hence, these two are very important to characterize the vibronic coupling, which modifies the electronic states by molecular vibration.

In the present work, vibrational real-time spectroscopy was applied to a derivative of thiophene oligomer with two quinoid thiophenes as an extension of previous works on thiophene derivatives [27]–[29]. The time-resolved spectrum after ultrashort pulse excitation revealed fine structures of instantaneous vibronic transition. The vibronic structure was found to be composed of several peaks associated with induced absorption. The energies and intensities of the vibronic transition peaks have been found to be correlated in the present paper. This finding can be usefully applied to the study of molecular vibronic structure both in the ground state and in the excited states.

2. Experiment

The sample molecule used in the present study is a novel synthesized quinoidal thiophene derivative with two thiophene rings, abbreviated as QT2 [30, 31]. The inset in figure 1 shows the molecular structure of this thiophene substitute. The concentration of QT2 sample in tetrahydrofuran solution was 1.5×10^{-4} mol dm^{-3}, which gave an optical density of 1.6 at the absorption peak around 690 nm (1.798 eV) in a 1 mm thick quartz cell.

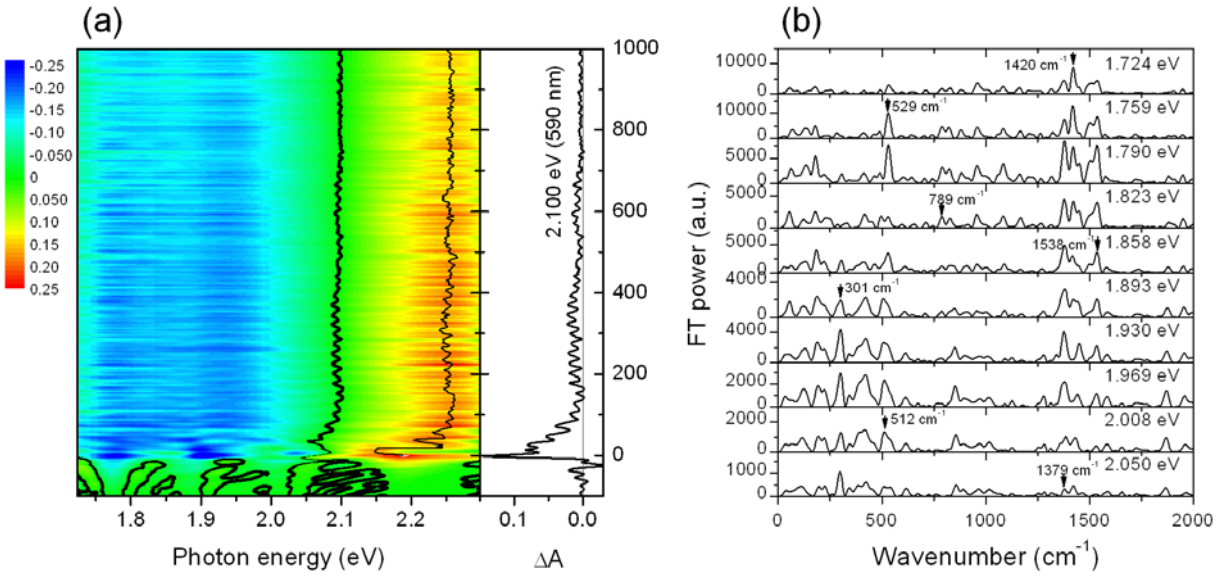

Figure 2. (a) The two-dimensional real-time absorbance change spectrum of QT2. Thick and thin solid lines indicate the photon energies where the value of the transient absorbance is zero and maximum, respectively. (b) FT power spectra at ten different probe photon energies.

The stationary absorption spectrum of QT2 was recorded with an absorption spectrometer (Shimadzu, UV-3101PC). The pulsed light source is a non-collinear optical parametric amplifier (NOPA) seeded by a white-light continuum [7]–[11]. The output from the NOPA was compressed to a Fourier-transform (FT) limited pulse with the duration of 6.7 fs. The output pulse from the NOPA with the spectral range of 535–725 nm was split into two beams as the pump and probe pulses, energies of which were about 45 and 5 nJ, respectively. The pump–probe signal was recorded from −200 to 2000 fs with a 1 fs step for the pump–probe delay time-range. The entire experiment was performed at room temperature (293 ± 1 K).

3. Results and discussion

3.1. Stationary spectra and real-time absorbance change

The absorption spectrum of the sample QT2 and the laser spectrum are shown in figure 1(a). The sample molecule has an absorption peak at 1.79 eV and two shoulders around 1.60 and 1.90 eV. Figure 1(b) shows the Raman spectrum pumped with an argon laser at 514.5 nm. There are three intense peaks at 907, 1392 and 1411 cm^{-1} and weak peaks at 1026, 1070, 1127, 1163 and 1244 cm^{-1} in the Raman spectrum.

The two-dimensional contour map of absorbance change $\Delta A(h\nu, t)$ is shown in figure 2(a) in the photon energy ($h\nu$) ranging from 1.72 to 2.35 eV at delay time (t) between −100 and 1000 fs. The thick solid line around 2.1 eV in figure 2(a) is the probe photon energy, $h\nu$, where the transient absorbance change ($\Delta A(h\nu, t)$) is zero at each delay time t. The thin solid line in the figure shows the intensity peak of absorbance change. A typical feature of the two-dimensional data is that the signals are negative and positive, respectively, in the lower and higher photon-energy regions except for some noise around 2.35 eV in all the delay time

ranges because of relatively weak transmitted probe light. The frequency ν of $\Delta A(h\nu)$ peak at the probe-photon energy range higher than 2.1 eV is located around 2.25 eV as shown in figure 2(a). While in the probe photon-energy range of the $\Delta A(h\nu)$ spectrum lower than about 2.1 eV, photon-energy and intensity of the peak are oscillating with time. From features of the oscillation, the molecular vibrational properties in this photon-energy range will be classified later in the present paper.

3.2. Mode assignment

The 128-channel delay time (t) dependent absorbance changes ($\Delta A(t)$) shown in figure 2(a) are temporally modulated. The time-dependent $\Delta A(t)$ is called the real-time trace hereafter. It provides information on the transition probability change associated with the wave packet motion on the PES prepared by the 6.7 fs pump pulses: one example of the real-time traces at 2.10 eV (590 nm) is shown on the right-hand side of figure 2(a). The cosine fast FT of $\Delta A(t)$ was performed in the time-range from 0 to 2000 fs. Ten examples of the FT results are shown in figure 2(b). Many vibrational modes are found in the FT power spectra, which were compared with the Raman scattering spectrum shown in figure 1(b). Because of a cut-off filter (532 nm) used in the Raman experiment, only signals above 800 cm^{-1} could be observed, while the FT of the real-time vibrational spectra show many modes with lower frequency than 800 cm^{-1}.

The limit will be relaxed with the use of a more appropriate filter, but it is difficult to go beyond 200 cm^{-1}. While in the case of the vibrational real-time spectroscopy upper and lower limits are determined by the duration of the pulse and the longest delay time, respectively. In the recent case, the highest and the lowest frequencies to be detected are, respectively, 2500 and 67 cm^{-1}, which correspond to twice the pulse duration and a quarter of the longest decay time. The former allows the simultaneous coherent excitation of at least two vibrational levels and the latter allows the observation of four oscillations of signal due to the relevant molecular vibration within the probing time. In principle, there is no limitation to the lowest frequency except the stabilities of the laser and sample to be studied. This indicates that vibrational real-time spectroscopy is superior to Raman spectroscopy for low-frequency modes, especially with very low frequency. Even more advantageously, it can provide vibrational phase with respect to zero delay time between the pump pulse and probe pulse. The phase relations among the vibrational modes may give the coupling mechanism among the modes.

Seven most intense modes were chosen from the FT power spectra and are listed in table 1 with the information of vibrational phase, coupling photon-energy range, classification of energy state and vibrational mode assignment. The vibrational phases in the case of vibrationally resonant excitation of molecules as in the present experiment, the wave packet motion in the ground state and the resonantly excited state give the sinusoidal and cosinusoidal oscillations, respectively, of the vibronic transition probabilities [32]–[36]. From the phase analysis, it was found that all of them are due to the mixed contributions of the wave packet motion in both the ground and excited states. Among them, modes of 301, 1420 and 1539 cm^{-1} are mainly from the ground state and the others are predominantly from the excited state except for the mode of 789 cm^{-1} with nearly equal contributions from both states.

The vibration assignment was performed according to the theoretical Raman modes calculated by the density functional theory (DFT) [37]–[39]. The relatively intense modes appearing in the FFT power spectra with frequencies of 789, 1379, 1420 and 1539 cm^{-1} were

Table 1. The frequencies, phases and photon energy ranges of the modes appearing in the FT spectra of the real-time trace and wave packet classification.

Modes (cm^{-1})	Cosine phase (π)	Photon energy range (eV)	Fraction of wave packet contribution (%)		Mode assignment by DFT
			Ground state	Excited state	
301	0.63	2.068–1.825	84	16	–
512	0.12	2.068–1.875	14	86	–
529	0.83	1.880–1.723	26	74	–
789	0.78	1.974–1.723	41	59	CH_2 scissoring
1379	−0.18	2.068–1.723	28	72	CH_3 vibration
1420	0.66	1.910–1.723	77	23	CH_2 twisting
1538	0.66	2.068–1.723	77	23	C=C asymmetric stretching

attributed to the CH_2 scissoring, CH_3 vibration, CH_2 twisting, and C=C asymmetric stretching, respectively. The modes with relatively low frequency are difficult to assign, but they are considered to be bending and/or torsion modes from their values. The results are listed in table 1.

3.3. Correlations among the vibration bands

3.3.1. Transient absorption spectrum and vibration band characterization. Figure 3(a) shows the three-dimensional time-resolved spectra observed in the delay time ranges from 100 to 200 fs in the photon-energy range lower than 2.10 eV. They show the periodical spectral change of the time-dependent difference absorption. The detection of these fine features has become possible by utilizing the combined system of extremely short pulse and ultra-broadband multi-channel detection system in the pump–probe experiment. In this way, the time-resolved spectrum gives a snap-shot of absorption spectra at the time when the relevant wave packet is located at some fixed point on the potential surface of the corresponding vibration mode. The obtained set of time-resolved spectra observed at the fixed point is considered to be the spectra projected from the n-mode potential hyper-surface to the $(n-1)$-mode potential hyper-surface. Therefore, a set of spectra taken at different snap-shot times will be useful for the determination of the multi-mode potential hyper surface landscape. This will be discussed elsewhere.

Here, we utilized another new analysis method, 'transition intensity and energy correlation of ΔA peaks', to analyze the very complicated features. The analysis is performed in the following way:

(1) The relatively featureless ΔA spectrum at the probe delay time of 50 fs ($\Delta A(h\nu)|_{t=50\,\mathrm{fs}}$) was selected to be the reference spectrum. This reference spectrum is shown in figure 3(b).

(2) The difference between $\Delta A(h\nu, t)$ and $\Delta A(h\nu)|_{t=50\,\mathrm{fs}}$ was calculated as the difference transient difference absorption spectrum ($D\Delta A(h\nu, t) = \Delta A(h\nu, t) - \Delta A(h\nu)|_{t=50\,\mathrm{fs}}$). In this process, the intensity of the reference $\Delta A(h\nu)|_{t=50\,\mathrm{fs}}$ was modified according to the electronic decay of the ΔA signal to adjust the distribution of the above-calculated difference ΔA around zero. The three-dimensional plot of $D\Delta A(h\nu, t)$ is shown in figures 3(c) with the probe delay time range from 100 to 200 fs.

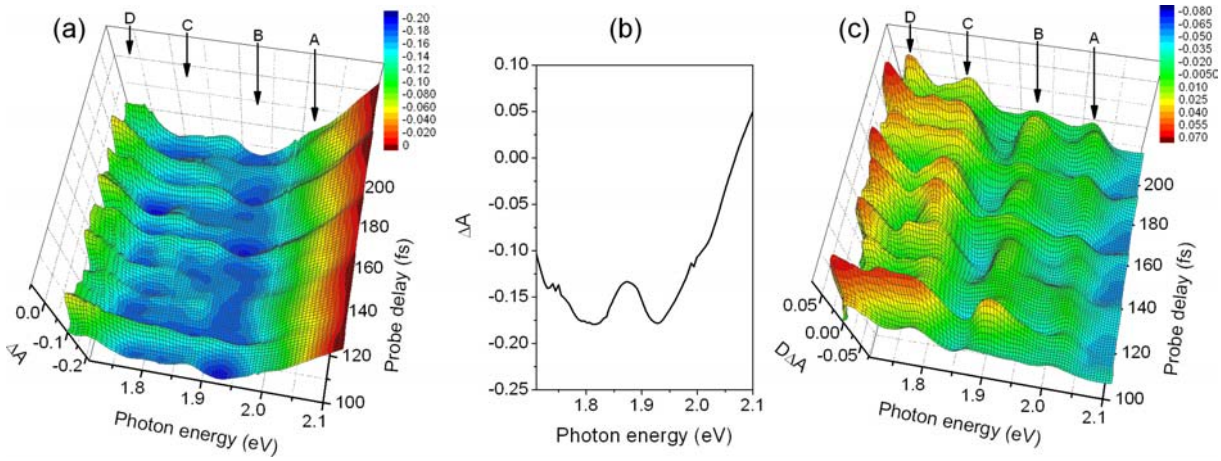

Figure 3. (a) Three-dimensional plots of difference absorbance ($\Delta A(h\nu, t)$; (b) difference absorbance at probe delay time 50 fs; (c) three-dimensional plots of transient difference absorbance ($D\Delta A(h\nu, t)$) spectra at a delay time from 100 to 200 fs. Symbols A, B, C and D with arrows in (c) represent the four prominent vibration peaks in the difference transient absorbance spectra.

(3) Four induced absorption peaks were found around 2.024, 1.921, 1.819 and 1.731 eV (referred to as peaks A, B, C and D, respectively) from the $D\Delta A(h\nu, t)$ spectra. By utilizing the *peak tracking method* [35] in the photon-energy range of 2.07–1.72 eV, the peak photon energy and the peak intensity of $D\Delta A(h\nu, t)$ were obtained as a function of probe delay time, results being shown in figure 4.

(4) The correlations among the four transition peaks were calculated using the following equation:

$$\rho_{xy} = \frac{\overline{(x(t) - \bar{x})(y(t) - \bar{y})}}{\sigma_x \sigma_y}.$$

Here, $x(t)$and $y(t)$ are the time-dependent variables to be correlated. $\bar{x}$ and $\bar{y}$ are the corresponding means, σ_x and σ_y are the standard deviations of the corresponding variables. The standard deviations of the traces of the tracking results and the correlation strengths among several peaks were calculated in the probe delay time range from 50 to 2000 fs, results being listed in table 2.

Comparing figure 3(a) with (c), it can be seen that four peaks are more prominent in figure 3(c) especially for peaks A and D which appear only as shoulders of transient difference absorbance spectra as shown in figure 3(a). This is because the $D\Delta A(h\nu, t)$ calculation subtracts the difference absorbance common to the relevant electronic states to which molecular vibration modes are coupled. The $D\Delta A$ can then provide the spectral change induced only by molecular vibration from some standard time (in this case, probe delay of 50 fs) without electronic contributions. This is because of very slow electronic dynamics in the present case of the thiophene oligomer with much longer lifetime than 1 ps [29]. Therefore, if the signal-to-noise ratio is high enough, as in the present study, $D\Delta A(h\nu, t)$ spectra are more effective than the transient absorbance to discuss the vibronic coupling of the vibrational mode to the transition.

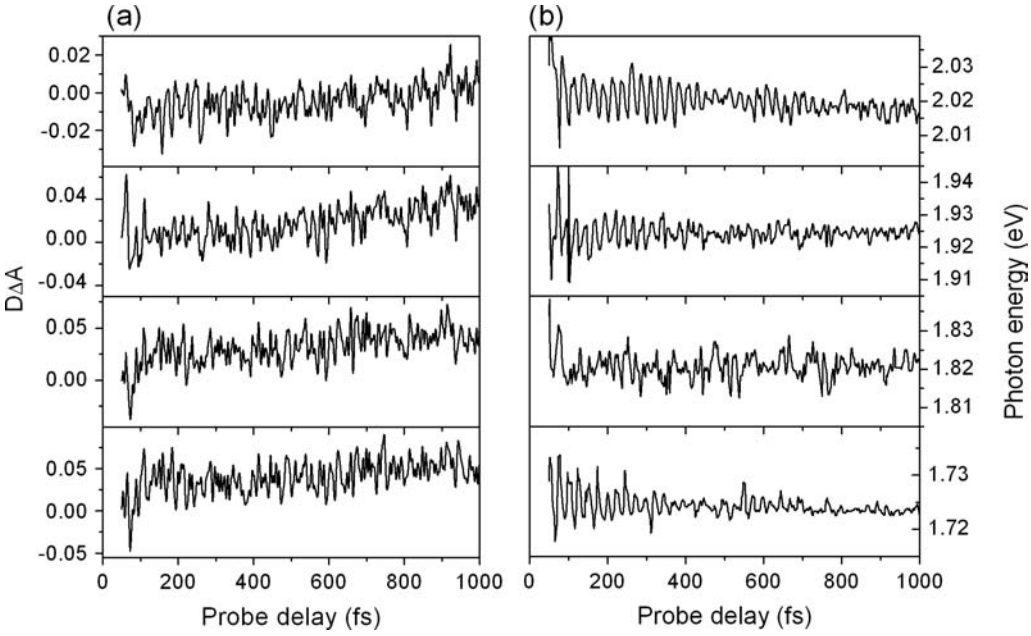

Figure 4. Probe delay time dependence of the photon energies (a) and the intensities (b) of the transient absorption peaks obtained by the peak tracking method. In (a) and (b), the traces for peaks A, B, C and D are plotted from top to bottom.

3.3.2. Correlation properties in the whole probe delay time range. From table 2(a), the peaks AB, BC, BD and CD have strong positive pairwise correlations and peaks AC and AD have relatively weak correlations, which means that all the transition intensities to the final vibronic states belonging to one electronic state are almost always simultaneously increasing or decreasing. This indicates the breakdown of the Condon approximation, because if the approximation is satisfied the transition probability integrated over the whole vibronic band must be maintained during molecular vibration as shown in the following. From Born–Oppenheimer approximation, the vibronic wavefunction in the ith state can be factorized into electronic function and nuclear wavefunction as follows:

$$|\Phi_i\,(q,\,Q)\rangle = |\phi_i\,(q,\,Q)\rangle\,\left|\chi_{i,m}\,(Q)\right\rangle, \quad (i = 1, 2;\, m : \text{integer, respecting the mode}). \tag{1}$$

Here, q and Q are the electron and nuclear coordinates, respectively. Thus, the transition dipole between these two states can also be factorized in the following way:

$$\langle\phi_1\,(q,\,Q)|\,eq\,|\phi_2\,(q,\,Q)\rangle_q\,\left\langle\chi_{1,m}\,(Q)\right|\chi_{2,m}\,(Q)\rangle_Q\,. \tag{2}$$

Here, the suffixes mean the variables to be integrated. This can be simplified under the Condon approximation

$$\langle\phi_1\,(q,\,Q_0)|\,eq\,|\phi_2\,(q,\,Q_0)\rangle_q\,\left\langle\chi_{1,m}\,(Q)\right|\chi_{2,m}\,(Q)\rangle_Q\,. \tag{3}$$

Q_0 is the nuclear coordinate at the equilibrium point. The integrated transition probability over Q could be expressed in the following equation:

$$\int P(Q)\,\mathrm{d}Q = \left|\langle\phi_1\,(q,\,Q_0)|\,eq\,|\phi_2\,(q,\,Q_0)\rangle_q\right|^2\left|\left\langle\chi_{1,m}\,(Q)\right|\chi_{2,m}\,(Q)\rangle_Q\right|^2. \tag{4}$$

Table 2. The correlation strengths among the corresponding photon energies and intensities of the difference transient absorption peaks. The terms PI and PPE mean the peak intensity and peak photon energy, respectively. std, standard deviation; cs, correlation strength; A, peak 2.024 eV; B, peak 1.921 eV; C, peak 1.819 eV and D, peak 1.731 eV.

(a) PI of IA peaks

	A	B	C	D
std	0.0084	0.0183	0.0202	0.0205
cs				
A		0.8214	0.4965	0.3517
B			0.8287	0.7522
C				0.9292
D				

(b) PPE of IA peaks

	A	B	C	D
std	0.0043	0.0025	0.0030	0.0020
cs				
A		0.1517	0.1915	−0.1075
B			0.2422	−0.0807
C				0.1042
D				

Therefore, under the Condon approximation, the first part of the right-hand side in equation (4) is independent of Q and comes out of the integral. The dynamic change in the transient absorption intensity is therefore concluded not due to the time-dependent Franck–Condon factor, which supports the constant integrated ΔA over the vibronic band. Instead, it is concluded to be due to the Herzberg–Teller mechanism [40, 41], revealing the third electronic state with which oscillation strengths are exchanged. This can be explained as follows.

In the Herzberg–Teller mechanism, as discussed in our previous paper [36, 37], the intensity of the transition being probed is modified by the change in the amounts of contributions of electronic states due to change in the molecular symmetry introduced by the molecular deformation during molecular vibration. Let us think of a three-level system composed of $\Phi_1(t)$, $\Phi_2(t)$ and $\Phi_3(t)$, of which wave packets are given by $\Psi_1(t)$, $\Psi_2(t)$ and $\Psi_3(t)$, respectively, when the molecule is in its equilibrium configuration. If it is deformed due to vibration then it can be given by

$$\begin{aligned}
\Phi_1(t) &= c_{1,1}(t)\Psi_1(t) + c_{2,1}(t)\Psi_2(t) + c_{3,1}(t)\Psi_3(t) \quad (\left|c_{1,1}(t)\right| \cong 1;\ \left|c_{2,1}(t)\right|, \left|c_{3,1}(t)\right| \ll 1),\\
\Phi_2(t) &= c_{1,2}(t)\Psi_1(t) + c_{2,2}(t)\Psi_2(t) + c_{3,2}(t)\Psi_3(t) \quad (\left|c_{2,2}(t)\right| \cong 1;\ \left|c_{1,2}(t)\right|, \left|c_{3,2}(t)\right| \ll 1),\\
\Phi_3(t) &= c_{1,3}(t)\Psi_1(t) + c_{2,3}(t)\Psi_2(t) + c_{3,3}(t)\Psi_3(t) \quad (\left|c_{3,3}(t)\right| \cong 1;\ \left|c_{1,3}(t)\right|, \left|c_{2,3}(t)\right| \ll 1).
\end{aligned} \tag{5}$$

$c_{x,y}(t)$ is the coefficient of the x state with respect to the y state, which has a periodic change with vibrational frequency of the mode in consideration. In this case none of the states $\Phi_1(t)$, $\Phi_2(t)$ and $\Phi_3(t)$ have a static dipole moment ($\mu_{11} = \mu_{22} = \mu_{33} = 0$), the transition dipole moment between $\Phi_1(t)$ and $\Phi_2(t)$, which is being probed, is given by

$$\begin{aligned}
\langle \Phi_1(t)|\, \mu \,|\Phi_2(t)\rangle &= c_{1,1}c^*_{2,2}\mu_{12} + c_{1,1}c^*_{3,2}\mu_{13} + c_{2,1}c^*_{1,2}\mu_{21} + c_{2,1}c^*_{3,2}\mu_{23} + c_{3,1}c^*_{1,2}\mu_{31} + c_{3,1}c^*_{2,2}\mu_{32}\\
&= (c_{1,1}c^*_{2,2} + c_{2,1}c^*_{1,2})\mu_{12} + (c_{1,1}c^*_{3,2} + c_{3,1}c^*_{1,2})\mu_{13} + (c_{2,1}c^*_{3,2} + c_{3,1}c^*_{2,2})\mu_{23}.
\end{aligned} \tag{6}$$

Here, the phase of the relevant wavefunctions was set for the dipole moment to be real. μ is the transition dipole operator between two electronic states. The phases of the wavefunctions were

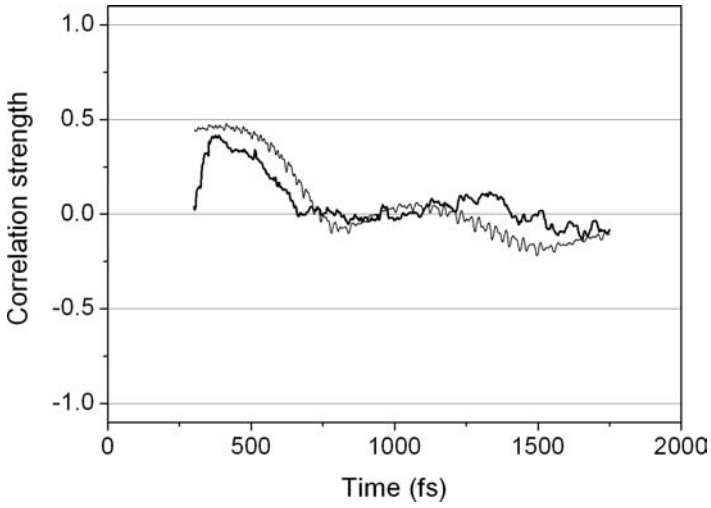

Figure 5. (a) Probe delay time dependence of correlations between the time-dependent photon energies of peaks A and B. The thick and solid lines depict the experimental results and the simulated results, respectively. A rectangular gate window with the full width of 300 fs was utilized during the calculation.

selected in such a way that the following are satisfied.

$$\begin{aligned} \mu_{12} &= \mu_{21} = \langle \Psi_1(t) | \, \mu \, | \Psi_2(t) \rangle \, , \\ \mu_{13} &= \mu_{31} = \langle \Psi_1(t) | \, \mu \, | \Psi_3(t) \rangle \, , \\ \mu_{23} &= \mu_{32} = \langle \Psi_2(t) | \, \mu \, | \Psi_3(t) \rangle \, . \end{aligned} \tag{7}$$

In the case that $c_{3,1}$ and $c_{3,2}$ are zero, there is no such effect of modulation due to the Herzberg–Teller mechanism. Therefore, the change indicates that there is a third state ($c_{3,1} \neq 0$, $c_{3,2} \neq 0$), which is mixed with $\Psi_1(t)$ and $\Psi_2(t)$ to form $\Phi_1(t)$ and $\Phi_2(t)$.

On the other hand, all of the correlation strengths of peak energies are not very high, as listed in table 2(b). There are two possible explanations for these low correlation strengths. One is that the correlation between any pair of traces is very weak at any probe delay time. The other is that the correlation strength between any pair of the traces is time-dependent; it has different values at different probe delay times. Therefore, the time dependence of the correlations is the key point to solve this problem, which is discussed in detail in the following subsection.

3.3.3. Time dependence of the correlation among the vibronic bands. In this subsection, the time dependence of the correlation property of the vibration bands is discussed. In figure 4(b), the photon energy traces of the neighboring peaks A and B have clear vibration feature, so these two traces were studied as an example to discuss the time-dependent correlation intensity. With a rectangular gate window of 300 fs width, the time-dependent correlation strength was calculated. Because of the width of the gate function, the correlation intensity was calculated in the limited delay time range of 200–1750 fs. The correlation trace shown in figure 5 is positive at a time shorter than 600 fs and then it gradually decreases to nearly zero. It may be explained by the following two mechanisms.

One is that the photon energies of the peaks A and B are correlated with each other in a shorter time range than 600 fs and after that the spectral shift of peaks A and B become uncorrelated resulting in zero correlation strength. The other possible mechanism is that it can

Table 3. The parameters of the vibrational signals for the calculation of time-dependent correlation strength. a, vibration amplitude; τ, vibrational phase relaxation time constant; ω, vibrational frequency in wavenumber and φ, cosine vibrational phase.

Peak A				Peak B			
a	τ (fs)	ω (cm^{-1})	φ (π)	a	τ (fs)	ω (cm^{-1})	φ (π)
1	500	301	−0.92	1	500	301	0.28
4.5	500	1379	0.78	3.6	200	1379	0.42
3.2	500	1420	−0.15	2.5	200	1420	−0.35

be a mixed contribution from several modes with different correlation strengths. To compare these two possibilities, the following analysis was performed.

To discuss the time-dependent correlation, it is important to determine the contributions of the vibrational coupling to peaks A and B. The FT results listed in table 1 and the FT results of the photon energy traces of peaks A and B were utilized to determine the vibration modes. The results show that three relatively intense modes of 301, 1379 and 1420 cm^{-1} are in action for the peaks A and B. The vibration parameters, such as the vibrational amplitude, exponential decay constant and vibrational phase, were determined by the spectrogram and FT analysis of the peak position traces of A and B, results being listed in table 3. Considering the experimental and calculation error, the precision of the decay time is set to the nearest hundred. With these results, the photon energy traces of peaks A and B could be reproduced and the corresponding correlation strength calculated is shown in figure 4(b). The simulated curve reproduced the experimental one relatively well.

From the phases of the vibration modes, modes of 1379 and 1420 cm^{-1} have positive correlations between peaks A and B. Concerning the mode of 301 cm^{-1}, peaks A and B are anti-correlated. Therefore, the nearly zero correlation strength at longer delay time than 600 fs can be attributed to the cancellation of the abovementioned positive and negative correlations. The fast decay of the positive correlation within the delay time of 600 fs can be explained in the following way. The positive correlation data are because of the more intense positive correlation strength than that of the negative one, and the fast decay is from the fast decay time of 1379 and 1420 cm^{-1} modes shown in the trace of peak B. Therefore, it is difficult to determine which of the two mechanisms is the case at present. Further study is needed to identify the origin of the time-dependent correlation intensity.

4. Conclusion

In conclusion, with the use of a short pulse, detailed structure could be found in the time-resolved spectrum. This vibronic structure cannot be observed in the low time-resolution spectrum. It means that the snap-shot spectrum is disclosing the vibronic spectrum instantaneously by *freezing* the molecular vibration within 6.7 fs of the probe pulse duration. The peak tracking method revealed four vibronic transitions buried in the time-integrated spectra over several vibrational periods of typical molecular vibration. Four vibronic transitions were found to be correlated among themselves with respect to the photon energies and intensities of

the peaks in the $D\Delta A(h\nu, t)$ spectra. It was shown that from the sign and size of the correlation, the vibronic coupling mechanism can be clarified. By studying the correlations, spectral features are expected to provide the potential hyper-surface landscape from the degrees of correlation between different vibrational modes.

Acknowledgments

We are grateful to Professor Emeritus Tetsuo Otsubo of Hiroshima University for providing us the QT2 molecule and Professor Eiji Tokunaga for his help in the Raman scattering measurement. We also thank Dr Izumi Iwakura for the DFT calculation of Raman modes and Information Technology Center of the University of Electro-Communications for supporting the computers during the calculation. This work was partly supported by the grant MOE ATU program in NCTU. A part of this work was also performed under the joint research project of the Laser Engineering, Osaka University under contract subject B1-27.

References

[1] Ergler Th, Rudenko A, Feuerstein B, Zrost K, Schroter C D, Moshammer R and Ullrich J 2006 *Phys. Rev. Lett.* **97** 193001
[2] Feuerstein B, Ergler Th, Rudenko A, Zrost K, Schroter C D, Moshammer R, Ullrich Niederhausen T and Thumm U 2007 *Phys. Rev. Lett.* **99** 153002
[3] Ha J, Maris M, Risen W, Tauc J, Thomson C and Vardeny Z 1986 *Phys. Rev. Lett.* **57** 3302
[4] Ruhman S, Joly A G, Kohler B, Williams L R and Nelson K A 1987 *Rev. Phys. Appl.* **22** 1717
[5] Mlynek J and Lange W 1979 *Opt. Commun.* **30** 337
[6] Harde H, Burggraf H, Mlynek J and Lange W 1981 *Opt. Lett.* **6** 290
[7] Shirakawa A, Sakane I and Kobayashi T 1998 *Opt. Lett.* **23** 1292
[8] Shirakawa A, Sakane I, Takasaka M and Kobayashi T 1999 *Appl. Phys. Lett.* **74** 2268
[9] Kobayashi T and Shirakawa A 2000 *Appl. Phys.* B **70** S239
[10] Baltuska A and Kobayashi T 2002 *Appl. Phys.* B **75** 427
[11] Baltuska A, Fuji T and Kobayashi T 2002 *Opt. Lett.* **27** 306
[12] Yamashita M, Yamane K and Morita R 2006 *IEEE J. Sel. Top. Quantum Electron.* **12** 213
[13] Gerullo G, Nisoli M, Stagira S, De Silvestri S, Tempea G, Krausz F and Ferencz K 1999 *Opt. Lett.* **24** 1529
[14] Apolonski A, Poppe A, Tempea G, Spielmann Ch, Udem Th, Holzwarth R, Hansh T W and Frausz F 2000 *Phys. Rev. Lett.* **85** 740
[15] Baum P, Lochbrunner S, Gallmann L, Steinmeyer G, Keller U and Riedle E 2002 *Appl. Phys.* B **74** S219
[16] Baum P, Lochbrunner S and Riedle E 2004 *Opt. Lett.* **29** 1686
[17] Gerullo G, Lanzani G, Muccini M, Taliani C and De Silvestri S 1999 *Phys. Rev. Lett.* **83** 231
[18] Kobayashi T and Shirakawa A 2000 *Chem. Phys. Lett.* **321** 385
[19] Kobayashi T, Saito T and Ohtani H 2001 *Nature* **414** 531
[20] Cinelli R A G, Tozzini V, Pellegrini V, Beltram F, Cerullo G, Zavelani-Rossi M, De Silvestri S, Tyagi M and Giacca M 2001 *Phys. Rev. Lett.* **86** 3439
[21] Adachi S, Kobryanskii V M and Kobayashi T 2002 *Phys. Rev. Lett.* **89** 27401
[22] Gerullo G, Leur L, Manzoni C, De Silvestri S, Shoshana O and Ruhman S 2003 *J. Phys. Chem.* A **107** 8339
[23] Bruno L 2004 *C. R. Physique* **5** 215
[24] Ishii N, Tokunaga E, Adachi S, Kimura T, Matsuda H and Kobayashi T 2004 *Phys. Rev.* A **70** 023811
[25] Gustafsson G, Cao Y, Treacy G M, Flavetter F, Colinari N and Heeger A J 1992 *Nature* **357** 477
[26] Burroughes J H, Bradley D D C, Brown A R, Marks R N, Mackay K, Friend R H, Burns P L and Holmes A B 1990 *Nature* **347** 539

[27] Kobayashi T, Wang H, Wang Z and Otsubo T 2006 *Chem. Phys. Lett.* **426** 105
[28] Kobayashi T, Wang H, Wang Z and Otsubo T 2006 *J. Chem. Phys.* **125** 044103
[29] Kobayashi T, Wang Z and Otsubo T 2007 *J. Phys. Chem.* A **111** 12985
[30] Takahashi T, Takimiya K, Otsubo T and Aso Y 2005 *Org. Lett.* **7** 4313
[31] Takahashi T, Matsuoka K, Takimiya K, Otsubo T and Aso Y 2005 *J. Am. Chem. Soc.* **27** 8928
[32] Kumar A T N, Rosca F, Widom A and Champion P M 2001 *J. Chem. Phys.* **114** 701
[33] Kumar A T N, Rosca F, Widom A and Champion P M 2001 *J. Chem. Phys.* **114** 6795
[34] Ishii N, Tokunaga E, Adachi S, Kimura T, Matsuda H and Kobayashi T 2004 *Phys. Rev.* A **70** 023811
[35] Ikuta M, Yuasa Y, Kimura T, Matsuda H and Kobayashi T 2004 *Phys. Rev.* B **70** 214301
[36] Yuasa Y, Ikuta M, Kobayashi T, Kimura T and Matsuda H 2005 *Phys. Rev.* B **72** 134302
[37] Becke A D 1993 *J. Chem. Phys.* **98** 5648
[38] Lee C, Yang W and Parr R G 1988 *Phys. Rev.* B **37** 785
[39] Frisch M J *et al* 2004 *Gaussian 03, Revision D.02* (Wallingford, CT: Gaussian, Inc.,)
[40] Kano H, Saito T and Kobayashi T 2002 *J. Phys. Chem.* A **106** 3445
[41] Kano H, Saito T and Kobayashi T 2001 *J. Phys. Chem.* B **105** 413